J|A|C|S
ARTICLES
Published on Web 01/10/2006

Switchable Surface Properties through the Electrochemical or Biocatalytic Generation of Ag^0 Nanoclusters on Monolayer-Functionalized Electrodes

Michael Riskin,[†] Bernhard Basnar,[†] Vladimir I. Chegel,[†,§] Eugenii Katz,[†] Itamar Willner,*[,†] Feng Shi,[‡] and Xi Zhang[‡]

Contribution from the Institute of Chemistry, The Hebrew University of Jerusalem, Jerusalem 91904, Israel, and the Key Laboratory of Organic Optoelectronics and Molecular Engineering, Department of Chemistry, Tsinghua University, Beijing, 100084, China

Received September 6, 2005; E-mail: willnea@vms.huji.ac.il.

Abstract: The electroswitchable and the biocatalytic/electrochemical switchable interfacial properties of a Ag^+−biphenyldithiol (BPDT) monolayer associated with a Au surface are described. Upon the application of a potential corresponding to −0.2 V the Ag^+−BPDT is reduced to the Ag^0−BPDT interface, and silver nanoclusters are generated on the interface. The application of a potential that corresponds to 0.2 V reoxidizes the monolayer to the Ag^+−BPDT monolayer. The reversible electrochemical transformation of the Ag^+−BPDT monolayer and of the Ag^0−BPDT surface was followed by electrochemical means and surface plasmon resonance spectroscopy (SPR). The SPR experiments enabled us to follow the kinetics of nanoclustering of Ag^0 on the surface. The hydrophobic/hydrophilic properties of the surface are controlled by the electrochemically induced transformation of the interface between the Ag^+−BPDT and Ag^0−BPDT states. The Ag^0−BPDT monolayer reveals enhanced hydrophilicity. The hydrophobic/hydrophilic properties of the interface were probed by contact angle measurements and force interactions with a hydrophobically-functionalized AFM tip. The Ag^0−BPDT interface was also biocatalytically generated using alkaline phosphatase, AlkPh, and *p*-aminophenyl phosphate as substrate. The biocatalytically generated *p*-aminophenol reduces Ag^+ ions associated with the surface to Ag^0 nanoclusters. This enables the cyclic biocatalytic/electrochemical control of the surface properties of the modified electrode.

Introduction

The control of the hydrophilic and hydrophobic properties of surfaces attracts substantial recent research activities.[1] Different applications of surface-regulated functions were suggested, including the development of self-cleaning surfaces,[2] sensors,[3] controlled delivery and transport,[4] and more.[5] The signal-triggered control of surface properties, and specifically, the reversible and cyclic regulation of the surface functions, attracts major interest. The electrochemical,[6] photochemical,[7] magnetic,[8] chemical,[9] and biocatalytic[10] activation of the surface properties was accomplished in recent years. For example, the redox activation of chemically modified electrodes between neutral and charged states was reported to reversibly switch the interface between hydrophobic and hydrophilic states, respectively.[6] Also, the electric field-induced bending of charged units tethered to electrodes by long-chain alkane units was employed to control the hydrophilic/hydrophobic properties of surfaces.[11] Recently, the electrochemically driven mechanical shuttling of molecular components on surfaces was used to control the hydrophilic/hydrophobic properties of surfaces, and the translation of molecular machinery into macroscopic mechanical events (movement of water droplets) was demonstrated in the system.[12] Several studies have addressed the wetting properties of nanoparticles associated with surfaces.[13] Superhydrophobic behavior of the lotus leaf structure was demonstrated with

[†] The Hebrew University of Jerusalem.
[‡] Tsinghua University.
[§] On leave from the Institute of Physics of Semiconductors, National Academy of Sciences of Ukraine, Kiev, Ukraine.

(1) Liu, Y.; Mu, L.; Liu, B.; Kong, J. *Chem. Eur. J.* **2005**, *11*, 2622−2631.
(2) (a) Wang, R.; Hashimoto, K.; Fujishima, A.; Chikuni, M.; Kojima, E.; Kitamura, A.; Shimohigoshi, M.; Watanabe, T. *Nature* **1997**, *388*, 431−432. (b) Feng, X. J.; Feng, L.; Jin, M. H.; Zhai, J.; Jiang, L.; Zhu, D. B. *J. Am. Chem. Soc.* **2004**, *126*, 62−63.
(3) (a) Liang, L.; Feng, X. D.; Liu, J.; Rieke, P. C. *J. Appl. Polym. Sci.* **1999**, *72*, 1−11. (b) Liang, L.; Feng, X. D.; Liu, J.; Rieke, P. C.; Fryxell, G. E. *Macromolecules* **1998**, *31*, 7845−7850. (c) Gabai, R.; Sallacan, N.; Chegel, V.; Bourenko, T.; Katz, E.; Willner, I. *J. Phys. Chem. B* **2001**, *105*, 8196−8202.
(4) Abbott, N. L.; Whitesides, G. M. *Langmuir* **1994**, *10*, 1493−1497.
(5) (a) Chia, S.; Cao, J.; Stoddart, J. F.; Zink, J. I. *Angew. Chem., Int. Ed.* **2001**, *40*, 2447−2451. (b) Liu, Y.; Mu, L.; Liu, B. H.; Zhang, S.; Yang, P. Y.; Kong, J. L. *Chem. Commun.* **2004**, 1194−1195. (c) Abbott, N. L.; Gorman, C. B.; Whitesides, G. M. *Langmuir* **1995**, *11*, 16−18. (d) Sun, T. L.; Wang, G. J.; Lin, F.; Biqian, L.; Yongmei, M.; Lei, J.; Zhu, D.-B. *Angew. Chem., Int. Ed.* **2004**, *43*, 357−360.
(6) Wang, X.; Katz, E.; Willner, I. *Electrochem. Commun.* **2003**, *5*, 814−818.
(7) Wang, X.; Zeevi, S.; Kharitonov, A. B.; Katz, E.; Willner, I. *Phys. Chem. Chem. Phys.* **2003**, *5*, 4236−4241.
(8) Katz, E.; Sheeney-Haj-Ichia, L.; Basnar, B.; Felner, I.; Willner, I. *Langmuir* **2004**, *20*, 9714−9719.
(9) Doron, A.; Katz, E.; Tao, G.; Willner, I. *Langmuir* **1997**, *13*, 1783−1790.
(10) Wang, X.; Gershman, Z.; Kharitonov, A. B.; Katz, E.; Willner, I. *Langmuir* **2003**, *19*, 5413−5420.
(11) (a) Lahann, J.; Mitragotri, S.; Tran, T.-N.; Kaido, H.; Sundaram, J.; Choi, I. S.; Hoffer, S.; Somorjai, G. A.; Langer, R. *Science* **2003**, *299*, 371−374. (b) Wang, X.; Kharitonov, A. B.; Katz, E.; Willner, I. *Chem. Commun.* **2003**, 1542−1543.
(12) Katz, E.; Lioubashevsky, O.; Willner, I. *J. Am. Chem. Soc.* **2004**, *126*, 15520−15532.

nanoparticle-functionalized interfaces, thus revealing the effects of nanoparticles on the wettability properties of the modified surfaces.

In the present study we report on the formation of a Ag^+-coated, densely packed, monolayer of an aromatic dithiol on Au supports and on the reversible control of the surface properties by the electrochemically induced generation and dissolution of Ag^0 nanoclusters.

Experimental Section

Chemicals. 4,4′-Biphenyldithiol (BPDT) was synthesized according to the published procedure.[14] All other chemicals were purchased from Aldrich or Sigma and used as supplied. Ultrapure water from a NANOpure Diamond (Barnstead) source was used throughout all the experiments.

Modification of Electrodes. A Au-coated (50 nm gold layer) glass plate (22×22 mm^2) (Analytical μ-Systems, Germany) was used as a working electrode. Prior to the modification, the Au surface was flame annealed in an *n*-butane flame for 5 min and cooled for 15 min under a weak stream of N_2. The BPDT monolayer was electrochemically deposited on a Au electrode according to the following procedure:[15a] A Au electrode was immersed in a BPDT solution, 1 mM, in 0.5 M KOH solution under N_2 atmosphere and preconditioned at -1.0 V for 5 min in order to obtain a thiol-free Au surface. The applied potential was swept to -0.4 V at a potential scan rate of 20 mV s^{-1}, and then the potential was held for 30 s at -0.4 V, resulting in the electrochemical anodic deposition of the BPDT monolayer. The BPDT-modified electrode was rinsed with water and soaked in 10 mM Ag_2SO_4 solution in 0.1 M H_2SO_4 overnight to yield a Ag^+ coating on the dithiol monolayer.

Electrochemical, Contact Angle, Surface Plasmon Resonance (SPR), Energy Dispersive Spectroscopy (EDS), Scanning Electron Microscopy (SEM), and Atomic Force Microscope (AFM) Measurements. The cyclic and linear sweep voltammetry experiments, as well as in situ measurements under constant applied potential on the modified electrode, were performed using an electrochemical PC-controlled analyzer−potentiostat IVIUM (PalmSens PC software). The chronoamperometric measurements were performed on an electrochemical analyzer (EG&G model 283) linked to a computer (EG&G software no. 270/250). In situ electrochemical measurements coupled with static contact angle measurements were performed on the modified Au-coated glass plates using a CAM2000 optical angle analyzer (KSV Instruments, Finland), and the PalmSens potentiostat. An aqueous droplet of ca. 20 μL of 0.1 M H_2SO_4 with the controlled diameter of the footprint of ca. 0.5 cm was deposited from a syringe on the modified surface (wired as a working electrode). Then, the counter electrode wire (Pt wire with a diameter of 0.1 mm) and the quasi-reference electrode (Ag wire with a diameter of 0.1 mm) were introduced into the droplet. All the potentials are reported versus the silver wire quasi-reference electrode, calibrated according to the relation $E_{Ag/AgCl(KCl,sat)} + 0.11\ V = E_{Ag-wire}$. Prior to contact angle measurement the droplet was kept under the applied potential for 5 min in order to allow it to reach the equilibrium shape. The images of the droplets were recorded, and each contact angle value was measured at least six times; the derived average contact angle values have a precision of $\pm 0.5°$. The Ag^+/BPDT/Au system was electrochemically reduced to generate Ag^0 nanoclusters associated with the modified surface and then oxidized back to the Ag^+ ionic state. These electrochemical processes were performed in the droplet upon measuring in situ the contact angles. Enzymatic reduction of Ag^+ was performed by immersing the Ag^+/BPDT/Au system in a buffer solution, pH = 7.0, of 50 mM glycine, 1 mM magnesium perchlorate ($Mg(ClO_4)_2$), and 1 mM magnesium sulfate ($MgSO_4$), containing 1 unit mL^{-1} of the enzyme alkaline phosphatase and 5 mM *p*-aminophenyl phosphate as the enzyme substrate. The latter was added in the dark and at the last moment, to prevent the feasible decomposition by visible light. After 1 h of reaction, the Au plate was taken out, rinsed with water, and dried with nitrogen, and the contact angle was measured ex situ using a 0.1 M H_2SO_4 droplet. Then the modified Au plate was oxidized for 5 min in 0.1 M H_2SO_4 under a constant potential of 0.2 V, rinsed with water, dried with nitrogen, and the contact angle was measured again in the same way.

The surface plasmon resonance (SPR) Kretschmann type spectrometer "NanoSPR" (light-emitting diode light source, $\lambda = 670$ nm) and the Au-coated glass slides, 0.4 cm^2 area exposed to the solution (Analytical μ-Systems, Germany), were used in this work. An auxiliary Pt electrode and a quasi-reference Ag electrode made from wires of 0.5 mm diameter were parts of the cell, thus allowing in situ electrochemical/SPR measurements upon stimulation of the electrochemical processes on the modified surface.

AFM measurements were performed using a SMENA-B atomic force microscope (NT-MDT, Russia) with a SMENA-A scanner head. Silicon cantilevers (CSC12, MikroMasch, Russia) with nominal spring constants of 0.03 and 0.05 N/m were modified with octadecyltrichlorosilane (OTS) by immersion into a 1% solution of OTS in toluene for 2 min, followed by subsequent rinsing with toluene, acetone, and ethanol, and blow drying with nitrogen. Samples were immersed into a 0.1 M Na_2SO_4 solution at a pH of 3 for the determination of the force curves. Deflection−distance curves were measured for each substrate on several (usually 3−4) 5×5 μm^2 sample spots, mapping the interaction between the tip and the sample on 225 points (15 by 15 data point mesh) on each of these areas. The obtained curves (between 675 and 900) were exported as ASCII files and further processed using Excel to extract the pull-off force for each individual curve. The SEM measurements were performed on the respective modified Au-coated glass plates using a UHR FEG SEM, model SIRION (FEI, U.S.A.), resolution 1.5 nm. The EDS analysis was performed on a EDAX spectrometer (Phoenix, AZ).

Results and Discussion

4,4′-Biphenyldithiol, BPDT (**1**), was assembled on a Au electrode using electrochemical oxidative deposition in a basic solution of **1**.[15] From the coulometric analysis of the linear sweep voltammogram obtained upon the BPDT adsorption (see Figure S1 in the Supporting Information), and assuming one-electron oxidative adsorption of the vertically oriented aromatic dithiols,[15d] eq 1, the surface coverage of the BPDT monolayer was estimated to be 0.82 nmole·cm^{-2}, which translates to a footprint of 20.2 Å^2 per molecule for **1**, which is close to the coverage of a densely packed BPDT monolayer.[15d] The resulting monolayer was then treated with Ag^+ to form the Ag^+−thiolate monolayer, Scheme 1. The resulting surface was rinsed to remove any nonspecifically adsorbed Ag^+ ions. Further studies of the resulting modified electrode were performed in the absence of Ag^+ ions in the bulk solution.

$$Au_{surf} + {}^{-}S-Ph-Ph-S^{-}{}_{sol} \rightarrow Au-S-Ph-Ph-S^{-}{}_{surf} + e^{-} \quad (1)$$

Figure 1A shows the cyclic voltammograms of the Ag^+-functionalized surface at different potential scan rates. The cyclic voltammograms reveal several important features: (i) A cathodic

(13) (a) Karuppuchamy, S.; Jeong, J. M. *Mater. Chem. Phys.* **2005**, *93*, 251−254. (b) Zhai, L.; Cebeci, F. C.; Cohen, R. E.; Rubner, M. F. *Nano Lett.* **2004**, *4*, 1349−1353.
(14) De Boer, B.; Meng, H.; Perepichka, D. F.; Zheng, J.; Frank, M. M.; Chabal, Y. J.; Bao, Z. *Langmuir* **2003**, *19*, 4272−4284.
(15) (a) Rifai, S.; Lafferrière, M.; Qu, D.; Wayner, D. D. M.; Wilde, C. P.; Morin, M. *J. Electroanal. Chem.* **2002**, *531*, 111−118. (b) Rifai, S.; Lopinski, G. P.; Ward, T.; Wayner, D. D. M.; Morin, M. *Langmuir* **2003**, *19*, 8916−8922. (c) Sabatani, E.; Cohen-Boulakia, J.; Bruening, M.; Rubinstein, I. *Langmuir* **1993**, *9*, 2974−2981. (d) Finklea, H. O. In *Electroanalytical Chemistry*; Bard, A., Ed.; Marcel Dekker: New York, 1996; pp 110−318

Scheme 1. Assembly of the Ag^+−Dithiol-Monolayer-Functionalized Electrode, and the Reversible Electrochemical Switching of the Interface between the Ag^+ Ionic State and the Ag^0 Nanoclusters

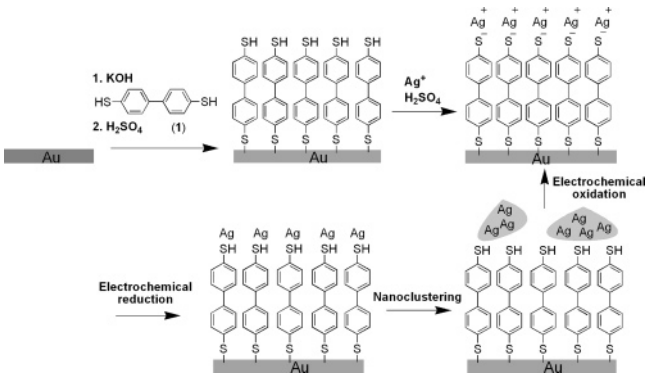

wave corresponding to the reduction of Ag^+ ions associated with the interface to Ag^0 is detected, and the corresponding oxidation wave of the metal is observed at positive potentials. The coulometric assay of the reduction (or oxidation) wave indicates that the surface coverage of the Ag^+/Ag^0 redox species corresponds to 0.82 nmole·cm^{-2}, suggesting that each BPDT unit is linked to a single Ag^+ ion and that the monolayer interface is completely saturated with the Ag^+ ions. (ii) The cyclic voltammograms reveal high stabilities upon cycling, implying that the reduction of Ag^+ or the oxidation of Ag^0 results in tightly bound surface species that are not dissolved or eliminated from the surface. (iii) The peak currents of the reduction or oxidation waves depend linearly on the scan rates implying that the redox-active species are surface confined (Figure 1A, inset). (iv) The cyclic voltammograms of the Ag^+-functionalized surface are not kinetically reversible and are characterized by large peak-to-peak separation. The cathodic and anodic waves reveal kinetic nonsymmetricity, reflected by nonsymmetrical shifts of the cathodic and anodic waves. The reduction wave of Ag^+ to Ag^0 is significantly shifted upon the increase of the potential scan rate, while the oxidation wave is almost unaffected upon increasing the scan rate. These results suggest that the reduction of Ag^+ to Ag^0 reveals slow electron-transfer kinetics at the surface, whereas the oxidation of the Ag^0-modified surface is fast. Therefore, the middle point potentials, $E_{1/2}$, of the cyclic voltammograms are different at various potential scan rates and they do not represent a thermodynamic potential of the redox system, E^0. Figure 1B shows the dependence of the cathodic and anodic peak potentials for the reduction and oxidation processes on the potential scan rate. Anodic and cathodic electron-transfer coefficients (α and β, respectively) were derived from the slopes of these dependences, and the ratio of α/β corresponds to 1/20. This kinetic nonsymmetricity of the electrochemical process does not allow the estimation of the electron-transfer rate constants by analyzing the cyclic voltammograms according to Laviron theory.[16] The crossing point of the two linear plots, extrapolated to slow potential scan rates, represents the thermodynamic potential for the redox process, E^0, and it corresponds to ca. 0.11 V.

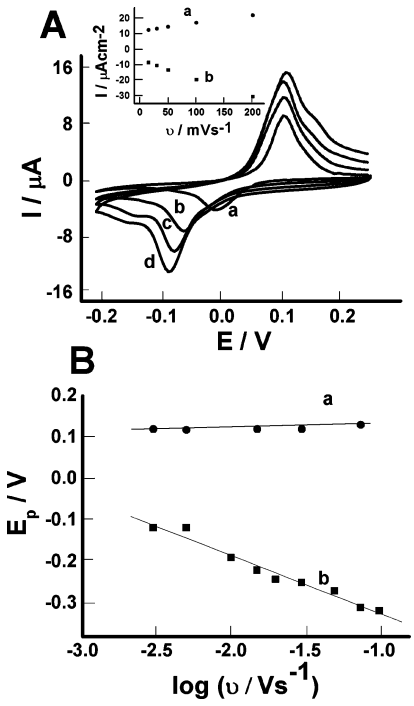

Figure 1. (A) Cyclic voltammograms of the Ag^+/BPDT/Au electrode recorded at different potential scan rates: (a) 5 mV s^{-1}, (b) 15 mV s^{-1}, (c) 30 mV s^{-1}, and (d) 50 mV s^{-1}. Inset: dependence of the anodic (a) and cathodic (b) peak currents of the cyclic voltammograms on the potential scan rate. (B) The dependence of anodic peak (a) and cathodic peak (b) potentials on the scan rate. The experiments were performed in 0.1 M H_2SO_4 under Ar.

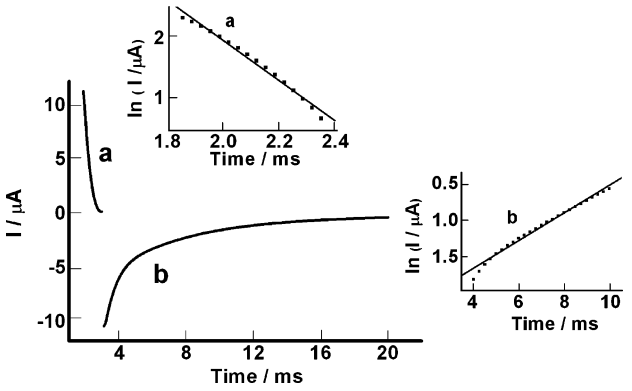

Figure 2. Chronoamperometric transients corresponding to the redox reactions of the $Ag^{+/0}$/BPDT/Au electrode upon the potential steps (a) from −0.2 to 0.2 V and (b) from 0.2 to −0.2 V. Insets: kinetic analysis of the current transients according to eq 2. The experiments were performed in 0.1 M H_2SO_4 under Ar.

Further support that the reduction of the Ag^+ and the oxidation of the resulting Ag^0 nanoclusters occur with different electrochemical kinetics was obtained from the chronoamperometric experiments. Figure 2 shows the cathodic transient, curve b, corresponding to the reduction of the Ag^+-functionalized monolayer and the anodic transient, curve a, corresponding to the oxidation of the Ag^0-modified surface upon application of the potential steps from 0.2 to −0.2 V and from −0.2 to 0.2 V, respectively. The results indicate a substantially faster process for the oxidation of the Ag^0 clusters. The experimental current transients replotted in semilogarithmic coordinates represent linear dependences with time, thus demonstrating monoexponential current decays characteristic for homogeneous redox monolayers.[17] Analysis of the current transients according to eq 2, where k_{et} corresponds to the interfacial electron transfer

(16) Laviron, E. *J. Electroanal. Chem.* **1979**, *101*, 19−28.
(17) (a) Forster, R. J.; Faulkner, L. R. *Anal. Chem.* **1995**, *67*, 1232−1239. (b) Forster, R. J. *Langmuir* **1995**, *11*, 2247−2255. (c) Forster, R. J. *Anal. Chem.* **1996**, *68*, 3143−3150. (d) Forster, R. J. *Analyst* **1996**, *121*, 733−741. (e) Katz, E.; Willner, I. *Langmuir* **1997**, *13*, 3364−3373.

and Q corresponds to the charge associated with the respective redox process of the surface-confined species[17] (Figure 2, insets), indicates that the electron-transfer rate constant for the reduction of Ag^+ is ca. 190 s^{-1} while the rate constant for the oxidation of the Ag^0 clusters corresponds to ca. 3360 s^{-1}. A possible explanation for the faster oxidation rate of the Ag^0 nanoclusters as compared to the reduction rate of the Ag^+−BPDT monolayer could be the rough structure of the Ag^0 nanoclusters. While the reduction of the Ag^+−BPDT structure requires overcoming the tunneling barrier of the BPDT monolayer, shortening of the electron-transfer distance for the oxidation of the Ag^0 nanoclusters through intramonolayer penetration of the rough nanoclusters could lead to the enhanced oxidation rate.

$$I(t) = k_{et}Q \exp(-k_{et}t) \quad (2)$$

The different rate constants derived from the chronoamperometric measurements are consistent with the nonsymmetrical shifts of the cathodic and anodic peaks in the cyclic voltammetry measurements observed upon increasing the potential scan rates. From the respective preexponential factors, $k_{et}Q$, and knowing the interfacial electron-transfer rate constants, k_{et}, for the reduction and oxidation processes, we calculated the charge, Q, associated with the reduction of the Ag^+ ions to Ag^0 clusters (or the oxidation of the Ag^0 clusters to Ag^+ ions). The charge associated with the Ag^+ units to Ag^0 translates to a surface coverage of 0.82 nmole·cm^{-2}, in excellent agreement with the surface coverage extracted by the coulometric assay of the cyclic voltammograms. Further support that the electrochemical reduction of the Ag^+−BDPT monolayer leads to the formation of Ag^0 nanoclusters on the BPDT monolayer is obtained by absorbance studies. The electrochemical transformation of the Ag^+−BDPT monolayer to the Ag^0−BDPT interface was followed on semitransparent Au-coated glass supports. The formation of the Ag^0−BDPT surface is accompanied with the appearance of an absorbance band at $\lambda = 469$ nm, consistent with the formation of Ag^0 nanoclusters[18] (see Figure S2 in the Supporting Information).

To further understand the electrochemically induced Ag^+ ion to Ag^0 metal transitions we applied in situ electrochemical-surface plasmon resonance (SPR) measurements. The coupling of the localized plasmon of the metal nanoparticles with the surface plasmon of the metal support is known to significantly affect the surface plasmon resonance spectrum, resulting in a shift in the minimum reflectivity angle and degeneration of the SPR spectra accompanied by the increase of the reflectance.[19] This physical effect was extensively used to amplify biorecognition events[20] and biocatalytic transformations[21] using Au or Ag nanoparticles as labels. Figure 3A depicts the time-dependent SPR spectra upon applying a potential step from $E = 0.2$ to $E = -0.2$ V on the Ag^+-functionalized monolayer. At the final potential, the Ag^+ ions are reduced to Ag^0. The process is

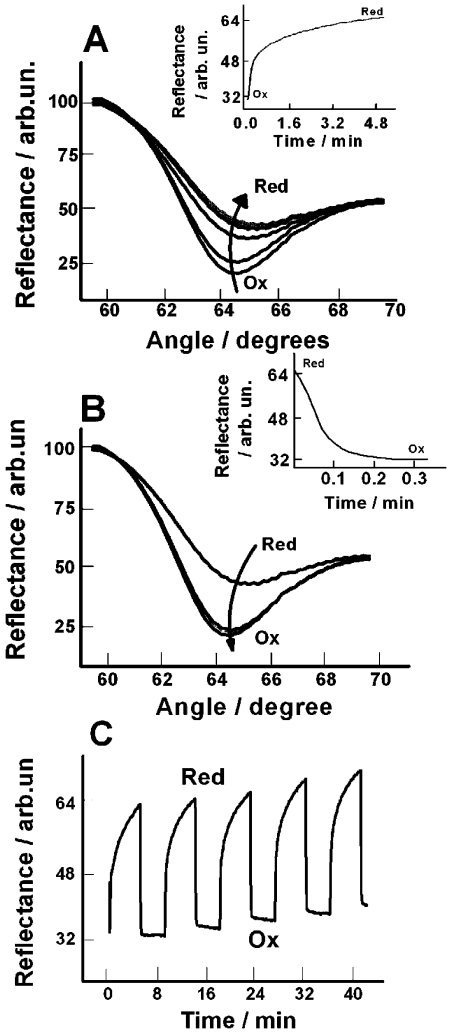

Figure 3. (A) SPR spectra of the $Ag^{+/0}$/BPDT/Au system at different time intervals after applying a potential step from 0.2 to −0.2 V. Inset: changes of the reflectance intensity of the modified electrode measured at a constant angle of 63.0° upon the potential step from 0.2 to −0.2 V. (B) SPR spectra of the $Ag^{+/0}$/BPDT/Au system at different time intervals after applying a potential step from −0.2 to 0.2 V. Inset: changes of the reflectance intensity of the modified electrode measured at a constant angle of 63.0° upon the potential step from −0.2 to 0.2 V. (C) Reversible changes of the reflectance intensity of the $Ag^{+/0}$/BPDT/Au system upon cyclic application of the potentials corresponding to −0.2 and 0.2 V on the modified electrode. The experiments were performed in 0.1 M H_2SO_4 under Ar. "Red" represents the system in the reduced state containing Ag^0 nanoclusters; "Ox" represents the system in the oxidized state containing Ag^+ ions.

accompanied by a shift of the minimum reflectivity angles to higher values and the observation of a shallower SPR curve. Similar changes were observed in the SPR spectra upon the reduction of the other metal ions to metal nanoclusters.[22] Figure 3A, inset, shows the time-dependent changes in the reflectance at a constant angle of 63.0°. The major time-dependent changes in the SPR spectra proceed for ca. 5 min. Interestingly, the time scale of chemical transformation occurring on the surface, and being probed by the SPR spectra, is by ca. 5 orders of magnitude slower than the primary electron transfer to Ag^+ that yields Ag^0, which proceeds on a time scale of ca. 15 ms, as elucidated by the chronoamperometry experiments. This apparent discrepancy may be resolved by realizing that the specific chemical

(18) Patil, V.; Sastry, M.; *Langmuir* **2000**, *16*, 2207−2212.
(19) (a) Lyon, L. A.; Musick, M. D.; Smith, P. C.; Reiss, B. D.; Pena, D. J.; Natan, M. J. *Sens. Actuatuators, B* **1999**, *54*, 118−124. (b) Lyon, L. A.; Pena, D. J.; Natan, M. J. *J. Phys. Chem. B* **1999**, *103*, 5826−5831. (c) Chah, S.; Hutter, S. E.; Roy, D.; Fendler, J. H.; Yi, *J. Chem. Phys.* **2001**, *272*, 127−128.
(20) (a) Lyon, L. A.; Musick, M. D.; Natan, M. J. *Anal. Chem.* **1998**, *70*, 5177−5183. (b) He, L.; Musick, M. D.; Nicewarner, S. R.; Sallinas, F. G.; Benkovic, S. J.; Natan, M. J.; Keating, C. D. *J. Am. Chem. Soc.* **2000**, *122*, 9071−9077.
(21) Zayats, M.; Pogorelova, S. P.; Kharitonov, A. B.; Lioubashevski, O.; Katz, E.; Willner, I. *Chem. Eur. J.* **2003**, *9*, 6108−6114.
(22) Chegel, V. I.; Raitman, O. A.; Lioubashevski, O.; Shirshov, Y.; Katz, E.; Willner, I. *Adv. Mater.* **2002**, *14*, 1549−1553.

transformations occurring on the surface and probed by the different electrochemical/optical means are different. The reduction of the Ag^+ ions to Ag^0 atoms proceeds rapidly on the electrode, and this process is, indeed, associated with the electron transfer and followed electrochemically. The migration of the Ag^0 atoms on the surface and their clustering is, however, a substantially slower process, Scheme 1. Since the SPR spectra follow the phenomenon of coupling between the localized plasmon of the nanoclusters and the Au-surface plasmon, the kinetics of nanoclustering of the Ag^0 atoms is optically probed. Figure 3B shows the SPR spectra observed upon the application of a potential step from −0.2 to 0.2 V on the Ag^0-nanocluster-modified electrode. A substantially faster change in the SPR spectra is observed, and the original SPR spectrum of the Ag^+-modified monolayer is reobtained. Figure 3B, inset, shows the time-dependent changes in the reflectance at a constant angle of 63.0°. The major time-dependent changes in the SPR spectra proceed within a time interval of ca. 20 s. Figure 3C shows the cyclic changes of the reflectance intensities (at 63.0°) upon the reversible switching of the monolayer configuration between the Ag^0 nanocluster and Ag^+ ion states, respectively. It should be noted that the alternate application of the potential values of −0.2 and 0.2 V on the BPDT-monolayer-functionalized Au electrode in the absence of the Ag^+/Ag^0 surface-confined redox system yields only a minute change in the minimum reflectivity angle, as well as in the reflectance intensities (see Figure S3 in the Supporting Information). Thus, the observed changes in the SPR spectra originate from the reversible Ag^0 nanocluster formation and dissolution, respectively. The enhanced declustering of the Ag^+ ions as compared to the clustering of the Ag^0 atoms may be attributed to the electrostatic repulsion of the Ag^+ ions generated upon the electrochemical oxidation of the clusters.

Figure 4A shows the SEM image of the Ag^+−BPDT-monolayer-modified Au electrode in comparison to the SEM image obtained after the reduction of the Ag^+−BPDT monolayer resulting in the formation of Ag^0 nanoclusters, Figure 4B. Clearly, dark spots of variable sizes in the range of 20−110 nm are observed, Figure 4B, that are attributed to the Ag^0 nanoclusters generated on the surface. The formation of these surface patterns is fully reversible, and the electrochemical oxidation of the Ag^0-modified electrode recovers the SEM image shown in Figure 4A. Further support that the dark spots in Figure 4B originate from Ag^0 nanoclusters is obtained from EDS measurements. Focusing the electron beam on the dark spots clearly indicates the spectral bands characteristic to Ag^0, Figure 4C, spectrum a. On the other hand, focusing the electron beam on bright domains of Figure 4B indicates that only trace signals of Ag^0, Figure 4C, spectrum b, are associated with these domains. It should be noted that with the available SEM resolution the existence of Ag^0 nanoclusters smaller than 3 nm cannot be excluded.

Different approaches to control the hydrophobicity of surfaces were discussed[13] including the preparation of rough surfaces coated with hydrophobic materials or the fabrication of ordered microstructured surfaces. The cyclic electrochemical transformation of the Ag^+−BPDT surface to the Ag^0-nanoclusters-modified interface suggests that the surface properties of the modified electrode might be reversibly altered. Figure 5A shows the in situ electrochemically stimulated contact angle changes

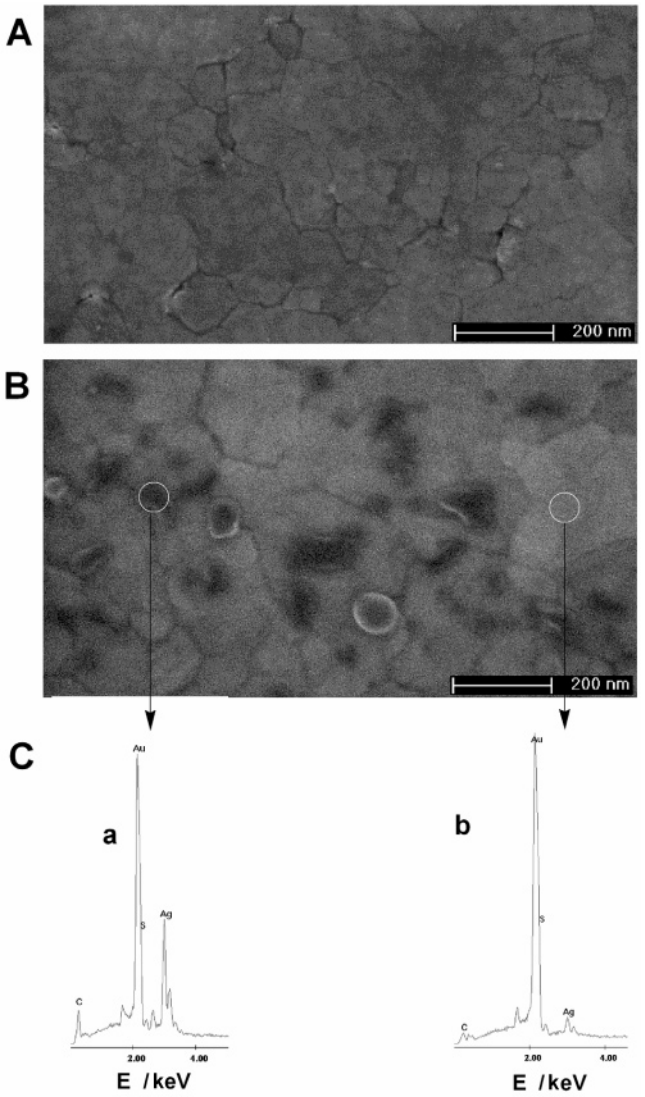

Figure 4. (A) SEM image of the Ag^+−BPDT-functionalized Au surface generated by the application of a potential corresponding to 0.2 V. (B) SEM image of the Ag^0-nanoclusters-modified surface generated by the application of a potential corresponding to −0.2 V. (C) EDS spectra corresponding to the analysis of the Ag^0−BPDT-nanostructured surface: (a) the dark domain of the SEM image; (b) the bright domain of the SEM image. The analyzed domains are indicated by circles.

of a H_2SO_4, 0.1 M, droplet upon cyclic switching of the potential on the electrode between −0.2 and 0.2 V. At an applied potential of −0.2 V, where the Ag^0 nanoclusters are present on the monolayer surface, the contact angle reveals a low value in the region of 48−52°. On the other hand, after applying a constant potential of +0.2 V, where the Ag^+ ions are linked to the monolayer interface, a high contact angle, corresponding to 64° ± 0.5° is observed. In a control experiment where the potential is cycled on the BPDT-modified electrode, that lacks the Ag^+ ions, between the values of −0.2 and + 0.2 V, minute changes, ≤±1°, in the contact angle of the 0.1 M H_2SO_4 droplet are observed. This implies that the potential-induced contact angle changes of the Ag^+-functionalized monolayer originate from the redox-stimulated reduction of the Ag^+ ions to the Ag^0 nanoclusters and the reverse dissolution of the nanoparticles. The Ag^0-nanocluster-modified interface reveals hydrophilic properties, while the Ag^+−thiolate monolayer interface exhibits,

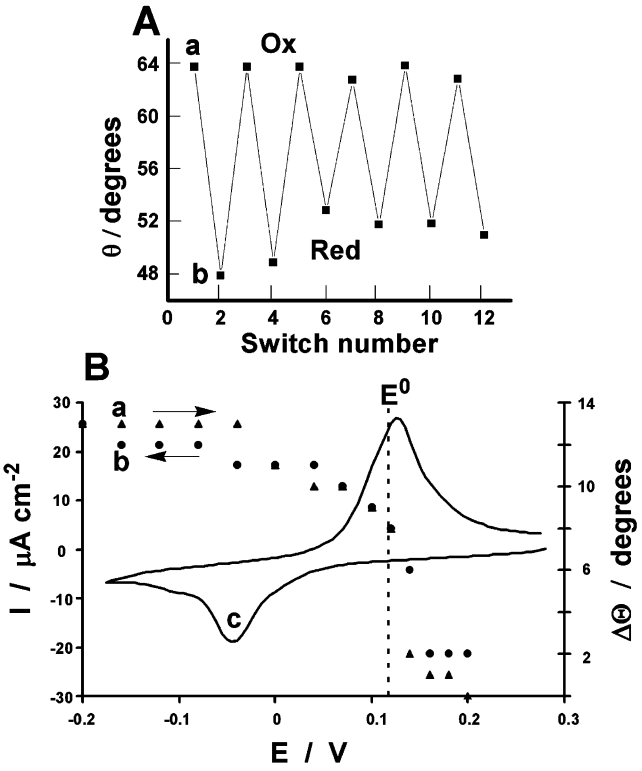

Figure 5. (A) Reversible changes of the contact angle of a 0.1 M H_2SO_4 aqueous droplet on the $Ag^{+/0}$/BPDT/Au system upon application of the potentials of (a) 0.2 V and (b) −0.2 V. The experiments were performed under Ar. At each point the measurement was performed after holding the system under the corresponding potential for 5 min. "Red" represents the system in the reduced state consisting of Ag^0 nanoclusters; "Ox" represents the system in the oxidized state consisting of Ag^+ ions. (B) Superposition of the potential-controlled in situ contact angle values of a 0.1 M H_2SO_4 droplet on the $Ag^{+/0}$/BPDT/Au system upon: (a) potential steps of 20−25 mV applied from −0.2 to +0.2 V; (b) potential steps of 20−25 mV applied from 0.2 to −0.2 V; (c) the cyclic voltammogram of the system obtained at the scan rate of 20 mV s^{-1} in 0.1 M H_2SO_4 aqueous solution.

based on the contact angle measurements, hydrophobic properties.

In further control experiments the contact angle features of the bare BPDT monolayer and of a Ag^0-saturated monolayer were examined. We find that the BPDT monolayer reveals a contact angle of ca. 79°, almost independent of the applied potential, indicating that this interface exhibits hydrophobic properties (this value is in accordance with the contact angle values of other densely packed dithiol monolayers[14]). The BPDT monolayer was saturated with Ag^0 nanoclusters by subjecting the Ag^+−BPDT monolayer to a potential of −0.2 V in the presence of Ag^+, 1×10^{-2} M, in 0.1 M H_2SO_4. The resulting interface exhibited a contact angle of 38−40°. Thus, the contact angle of the Ag^0-nanoclustered surface (that revealed enhanced hydrophilicity) generated by the electrochemical reduction of the Ag^+−BPDT monolayer is consistent with the contact angle of the saturated Ag^0-nanoclustered interface. As the Ag^0 nanoclusters formed by the reduction of the Ag^+−BPDT monolayer yield only a partially covered surface the hydrophilic properties are turned only in part.

Figure 5B, curve a, shows the contact angles of the 0.1 M H_2SO_4 droplet on the Ag^+ monolayer upon the stepwise alteration of the potential applied on the electrode from 0.2 to −0.2 V, by augmentation of the potential step value by 20−25 mV. A sharp decrease in the contact angle value is observed at ca. 0.11 V, consistent with the E^0 value derived from the electrochemical measurements for the reduction of the Ag^+−thiolate layer to the hydrophilic Ag^0 nanoclusters, Figure 5B, curve c. Figure 5B, curve b, shows the changes in the contact angle values of the 0.1 M H_2SO_4 aqueous droplet, positioned on the Ag^0−nanocluster interface, upon the stepwise change of the potential from −0.2 to 0.2 V. The contact angle characteristic to the Ag^0-nanoclustered electrode changes rapidly, and increases in its value most steeply, at an applied potential of 0.11 V, consistent with the formation of a hydrophobic interface upon the oxidation of the metal nanoclusters to the Ag^+−thiolate monolayer state. The contact angle measurements performed upon the stepwise potential changes in the opposite directions do not show any hysteresis; thus, the droplet is equilibrated with the modified interface on the time scale of the experiment, and the derived contact angle behavior superimposes the thermodynamic equilibrium corresponding to the potential-controlled redox state of the modified surface.

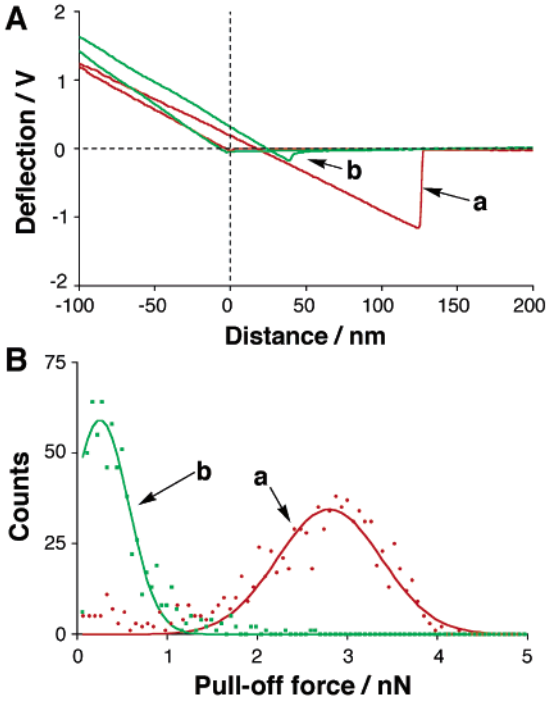

Figure 6. Force interaction between a hydrophobic AFM tip and the $Ag^{+/0}$ surface as a function of the oxidation state of Ag. (A) Typical deflection−distance curve on (a) Ag^+ and (b) Ag^0 surfaces in a 0.1 M Na_2SO_4 solution, pH = 3. (B) Distribution of the calculated pull-off force on (a) Ag^+ and (b) Ag^0 surfaces. The data points represent the frequency of occurrence of a specific pull-off force; the solid lines represent a Gaussian fit to these data.

Further support that the hydrophilic/hydrophobic properties of the interface are controlled by the redox transformation $Ag^+ + e^- \rightleftharpoons Ag^0$ is obtained from AFM force measurements that follow the affinity interaction between the hydrophobic-modified tip and the electrochemically triggered Ag^+−thiolate monolayer surface. Toward this goal, the Si-AFM tip was modified with octadecyltrichlorosilane (OTS) to yield a hydrophobic tip, and the force measurements were performed in 0.1 M Na_2SO_4, pH = 3. Figure 6A shows a typical force curve upon monitoring the Ag^+−thiolate-modified surface generated by the application of the potential of 0.2 V, curve a, and a representative force curve of the hydrophobic tip interacting with the Ag^0-nano-

Scheme 2. Biocatalytic Generation of the Ag^0 Nanoclusters on the Functionalized Surface, and Electrochemical Regeneration of Ag^+ Ions Associated with the Interface

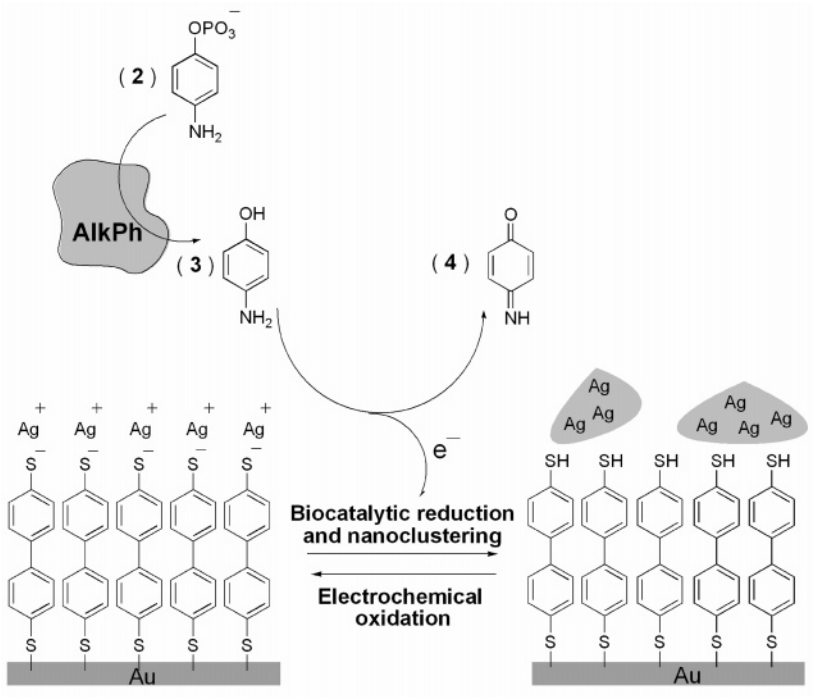

cluster-modified monolayer after applying a potential of −0.2 V, curve b. The detachment of the hydrophobic tip from the surface requires a force corresponding to 3.2 nN, whereas the disconnection of the hydrophobic tip from the Ag^0-nanocluster-modified interface, clearly, requires a substantially lower force corresponding to 0.5 nN. Such force interactions were recorded on 3−4 different domains of the Ag^+- or Ag^0-nanocluster-modified surfaces with a total statistics of 675−900 measurements for each monolayer state. Figure 6B shows the derived histograms. The results indicate that the interaction of the hydrophobic tip with the Ag^+−thiolate surface, which exhibits a hydrophobic character, results in high force interactions, average force ca. 2.8 nN, while the Ag^0 surface reveals lower affinity toward the hydrophobic tip, force centered at 0.3 nN, consistent with weak interactions between the hydrophilic surface and the hydrophobic tip. The selective force interactions between the modified electrode and the surface may be reversibly switched by the cyclic transformation of the interface between the Ag^+ and Ag^0-nanocluster states. It should be noted that although the SEM images indicate that the surface is only partially covered with the Ag^0 nanoclusters, the force experiments reveal a distinct decrease in the force interactions. This is attributed to the existence of small Ag^0 nanoclusters (<3 nm) in the apparently "bare" domains.

The success to reversibly switch the hydrophobic/hydrophilic properties of the Ag^+−thiolate monolayer by electrochemical means suggests that one may couple biocatalysis and electrochemistry to reversibly control the surface properties of the Ag^+−thiolate-modified surface, Scheme 2. Alkaline phosphatase hydrolyses *p*-aminophenyl phosphate (**2**) to *p*-aminophenol (**3**). The latter product acts as reducing agent, and it reduces Ag^+ to Ag^0 nanoclusters, with the concomitant formation of the imino−quinone type product (**4**). Thus, one might transform by a biocatalytic process, driven by alkaline phosphatase, the conversion of the Ag^+-thiolated interface to the hydrophilic Ag^0-nanocluster interface, and upon the electrochemical oxidation of the surface the hydrophobic Ag^+−thiolate layer would be regenerated, Scheme 2. Figure 7A shows the SPR spectrum of the Ag^+-thiolated monolayer prior to the interaction with alkaline phosphatase and **2**, curve a, and after treatment with the biocatalyst and **2**, curve b. The shift in the minimum reflectivity angle, and the shallow pattern of the reflectivity, are well consistent with the formation of the metal nanoclusters on the surface. Figure 7A, curve c, shows the SPR spectrum of the biocatalytically generated Ag^0-nanostructured interface after applying a potential step from −0.2 to 0.2 V. The SPR spectrum of the Ag^+−thiolate monolayer is regenerated, implying that

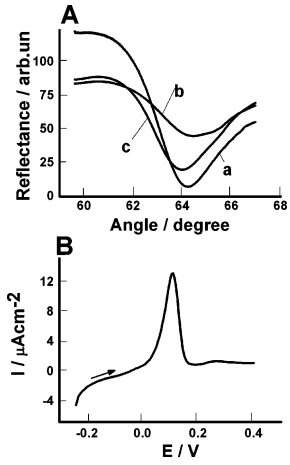

Figure 7. (A) SPR spectra corresponding to (a) the initial Ag^+−BPDT-monolayer-functionalized Au surface; (b) after the biocatalyzed reduction of the surface with alkaline phosphatase, 1 unit per mL, and **2**, 5 mM, for 1 h and the generation of Ag^0 nanoclusters on the surface; (c) after electrochemical oxidation of the Ag^0 nanoclusters and regeneration of the Ag^+−BPDT monolayer by applying a potential corresponding to 0.2 V. (B) Linear sweep voltammogram corresponding to the electrochemical oxidation of the biocatalytically generated Ag^0 nanoclusters. Potential scan rate, 20 mV s^{-1}.

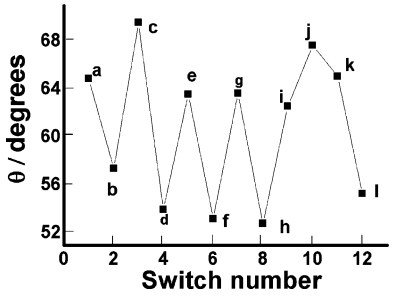

Figure 8. Reversible changes of the contact angle of a 0.1 M H_2SO_4 aqueous droplet on the $Ag^{+/0}$/BPDT/Au system upon biocatalytic reduction and electrochemical oxidation of the modified surface: (a) initial Ag^+−BPDT state; (b, d, f, h, and l) biocatalytically generated Ag^0−BPDT state in the presence of alkaline phosphatase, 1 unit per mL, and **2**, 5 mM; (c, e, g, and i) electrochemically oxidized Ag^+−BPDT state generated by applying a potential of 0.2 V; (j) control experiment in the presence of the Ag^+−BPDT state and alkaline phosphatase and absence of **2**; (k) control experiment in the presence of the Ag^+−BPDT state and **2**, 5 mM, and in the absence of alkaline phosphatase.

the potential step oxidized the Ag^0 nanostructures to the Ag^+ state. Figure 7B shows the linear sweep voltammogram of the alkaline phosphatase generated Ag^0-nanostructured interface upon scanning the potential from −0.25 to 0.4 V. The anodic wave indicates that the electrochemical oxidation of the Ag^0 nanoclusters, indeed, occurred. The coulometric analysis of the anodic wave indicates that the full coverage of the thiolated monolayer by Ag^+ ions was accomplished, implying that the enzyme transformed all the Ag^+−thiolate units to the Ag^0 nanoclusters.

Contact angle measurements further confirmed the cyclic transition of the interface from the hydrophobic Ag^+−thiolate layer generated by electrochemical means and the Ag^0-nanoclustered surface produced by the biocatalytic process, Figure 8. At point a, the monolayer exists in the hydrophobic Ag^+−thiolate state. The Ag^+−thiolate interface was then interacted with the biocatalytic alkaline phosphatase/**2** system, and the contact angle of the 0.1 M H_2SO_4 droplet was ex situ monitored on the resulting surface, point b. The lower contact angle value confirms the formation of the Ag^0 nanoclusters, that exhibit enhanced hydrophilicity. The in situ electrochemical oxidation of the surface under the 0.1 M H_2SO_4 droplet restores the hydrophobic interface, point c. The points d, f, and h represent the contact angle of the Ag^0−nanocluster interface attained by repeated biocatalytic transformations with alkaline phosphatase/**2**. At points e, g, and i, the Ag^+−thiolate monolayer was generated in situ by the electrochemical oxidation of the clusters, to the Ag^+−thiolate state. At points j and k, the Ag^+−thiolate layer is treated either with alkaline phosphatase, or with the substrate **2** only, respectively. The interface is not transformed into a hydrophilic state, implying that only the combination of alkaline phosphatase/**2** yields the hydrophilic surface. Indeed, treatment of the Ag^+−thiolate support with the alkaline phosphatase/**2** biocatalytic system regenerates the hydrophilic Ag^0-nanoclustered support, point l.

Conclusions

The present study has demonstrated the cyclic control of the hydrophilic/hydrophobic properties of a Ag^+−thiolate monolayer by electrochemical means. In addition to the control of the macroscopic surface properties of the Ag^+/Ag^0-functionalized interface, interesting nanometric phenomena related to the switchable functions of the surfaces were elucidated. We were able to follow the kinetics of interfacial electron transfer that lead to the reduction of the Ag^+−thiolate monolayer to the Ag^0 nanoclusters and to the oxidation of the Ag^0 nanoclusters to the Ag^+−thiolate interface. Most interesting was the kinetic elucidation of the 2D lateral clustering of the Ag^0 atoms on the thiolate monolayer. Also, the demonstration that the electrochemical reduction and oxidation of the Ag^+ and Ag^0 nanoclusters on the surface proceed laterally on a two-dimensional surface, without the diffusion of the component into the solution, is unique and noteworthy. Other metal ions, e.g., Hg^{2+}, Cd^{2+}, or Pb^{2+}, as well as other functional monolayers, such as carboxylic acid-terminated monolayers, are anticipated to yield similar electroswitchable surface properties.

A further paradigm that originates from this study involves the coupling of biocatalytic processes and electrochemistry for the cyclic and reversible control of the surface properties. This may be a valuable approach for the development of new sensors and delivery and controlled release systems.

Acknowledgment. This study is supported by the German−Israeli Program (DIP) and by the Israel Science Foundation.

Supporting Information Available: Linear sweep voltammogram showing the oxidative deposition of BPDT on a Au electrode, differential absorption spectrum of electrochemically generated Ag^0 nanoclusters on a BPDT/Au electrode, and SPR spectra obtained on the BPDT-monolayer electrode upon application of variable potentials. This material is available free of charge via the Internet at http://pubs.acs.org.

JA0561183